Available online at www.CivileJournal.org

Civil Engineering Journal

(E-ISSN: 2476-3055; ISSN: 2676-6957)

Vol. 11, No. 12, December, 2025

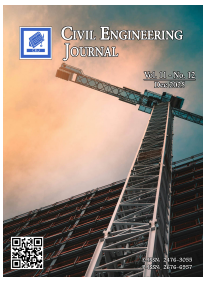

Experimental Study on Electrochemical Corrosion Law of Rebar Under Alternating Magnetic Field

Jianyu Yang [1], Xin Ye [2*], Weijun Yang [2]

[1] School of Hydraulic and Ocean Engineering, Changsha University of Science & Technology, Hunan 410114, China.

[2] School of Civil and Environmental Engineering, Changsha University of Science & Technology, Hunan 410114, China.

Received 17 August 2025; Revised 18 November 2025; Accepted 22 November 2025; Published 01 December 2025

Abstract

The alternating magnetic field (MF) environment of coastal substations and magnetic levitation systems generates strong electromagnetic interference, which may affect the corrosion behavior of rebars in concrete structures. To clarify the influence law of rebar corrosion when exposed to an alternating MF, an alternating MF simulation test device was designed and manufactured according to the principle of alternating electromagnetic induction. The macroscopic corrosion morphology and electrochemical corrosion characteristics of rebars under alternating MF of different intensities were investigated by accelerated corrosion tests, electrochemical tests and natural corrosion electrochemical tests. The corrosion behavior mechanism of rebars under alternating MF was revealed. The results show that: 1) The diffusion rate and concentration of corrosion products in the solution are proportional to the magnetic induction strength. The alternating MF accelerates rebar corrosion. 2) The E_{corr} of rebar shifts negatively with the magnetic induction strength increases, with a more pronounced shift in the early stage of corrosion than in the later stage. 3) Under the natural corrosion state, the 5 mT MF makes the open circuit potential (OCP) shift 12 mV negatively compared with that without MF. When the potential reaches 8mV, the passivation film begins to be destroyed. 4) The R_1 of rebar is inversely proportional to the magnetic induction strength.

Keywords: Alternating MF; Rebars; Corrosion; Electrochemistry; Magnetic Induction Strength.

1. Introduction

The ultra-large-scale maglev rail transit and substation have become an important engine to support the efficient operation of the city. Its low-carbon and high-speed development model is the core driving force for national energy transformation and urban construction [1-4]. During the operation of infrastructure such as magnetically suspended rail transit and substations, high-intensity alternating MF will continue to be generated [5, 6]. However, their impact on the electrochemical corrosion behavior of rebars in concrete is still inconclusive. Although some studies have investigated the effect of MF on metal corrosion [7, 8], the research on the effect of alternating MF on the corrosion behavior of rebars in concrete structures remains scarce. It is difficult to accurately evaluate the effect of alternating MF on the long-term performance of reinforced concrete structures in engineering practice. Therefore, it is very important to study the rebar corrosion caused by alternating MF.

Corrosion of rebars is the main cause of concrete durability degradation, leading to decreased mechanical properties of rebars and ultimately structural fatigue failure [9-11]. The existing research pays more attention to the corrosion rate and corrosion amount of rebars, but there are few studies on the mechanism of rebar corrosion behavior. Yang [12]

* Corresponding author: 2769339804@qq.com

http://dx.doi.org/10.28991/CEJ-2025-011-12-01

proposed a formula for calculating the corrosion rate per unit area of rebar corrosion caused by stray current and established a modified model of rebar corrosion based on the Nernst equation, Faraday's first law of electrolysis, and the law of conservation of mass and energy. On this basis, Li et al. [13] & Liu et al. [14] carried out research on the influence of corrosion behavior of rebars in different environments. Among them, Li's [13] research shows that the MF gradient force generated under the action of MF will protect the passivation film on the surface of rebars and inhibit the corrosion of rebars. Ye [15] further established the model of rebar corrosion under the action of MF. The experimental results showed that the model is closer to the observed value. The influence of the MF environment on the electrochemical reaction process has been an increasingly in-depth research field, but the relationship between MF and steel corrosion behavior remains poorly understood. Some studies have concluded that the constant MF has an inhibitory effect on the corrosion of rebars [16-18]. Other studies suggest that MF accelerates corrosion [19-22]. It is obvious that the MF has an impact on the corrosion behavior of rebars. However, the current research is almost considering a simpler constant MF, and there are few studies on the alternating MF under complex working conditions.

The influence of alternating MF on the rebars' corrosion behavior is still in the exploratory stage. Studies have shown that the greater the intensity and frequency of the alternating MF, the lower the concrete resistivity and the higher the rebar corrosion rate [23]. The rebar corrosion in concrete is susceptible to the influence of alternating MF [24–26]. The alternating strong magnetic force generated by the running maglev train causes the rebars in the track beam to generate magnetic flux and induced eddy current. The induced eddy current generates Joule heat, which increases the internal temperature of the main beam and leads to electrochemical corrosion [27]. It can be seen that the alternating MF is likely to be one of the influencing factors of steel corrosion.

Based on the principle of electromagnetic induction, this study will design an alternating MF generator and systematically study the effect of alternating MF on the corrosion behavior of rebars through the control variable method. The research content is divided into three parts: 1) Accelerated corrosion test of rebars under different MF strength and immersion time conditions; 2) Comparative test of electrochemical test under natural corrosion conditions; 3) By comparing and analyzing the electrochemical parameters such as corrosion potential, current density, and impedance spectrum, the electrochemical mechanism of alternating MF affecting the rebars' corrosion will be revealed. The process flowchart of methodology is shown in Figure 1.

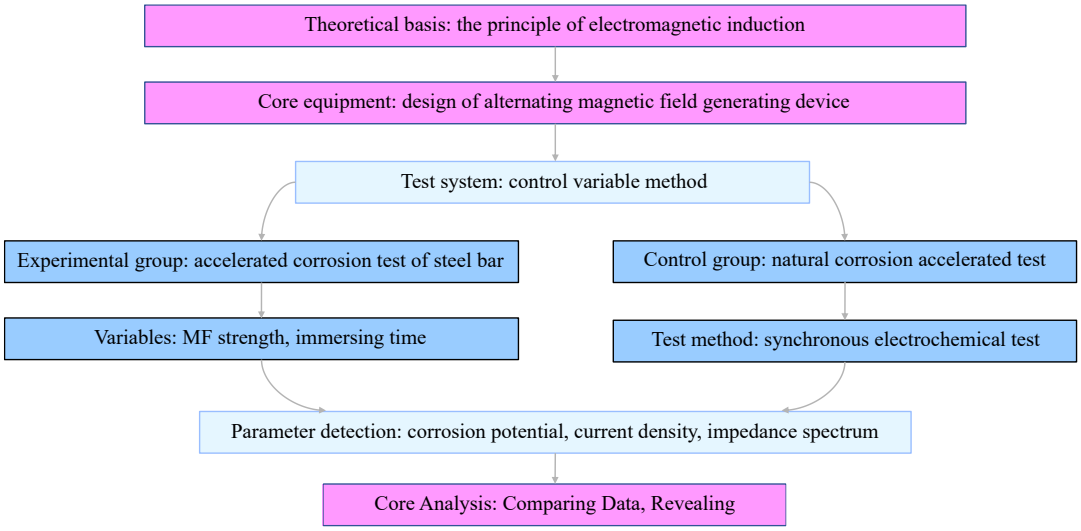

Figure 1. The process flowchart of methodology

2. Experimental

The alternating MF generator was composed of two identical and coaxial circular conductor coils. The coil diameter was 30 cm. The center distance of the two circles was controlled to be the radius of the coil. By applying alternating current in the same direction, a more uniform alternating MF was superimposed. The wire of the winding coil was copper enameled wire. The cross-sectional area was 2.5 mm^2. The number of turns was 300. The series sliding rheostat was 200 Ω. After the coil is energized by alternating current for 5 min, the magnetic induction strength of the radial center of the MF was measured by the milli-teslameter. A single variable method was adopted to control the magnitude of the magnetic induction by adjusting the alternating current, and the bars were subjected to alternating magnetic induction of 1 mT, 2 mT, 3 mT, 4 mT and 5 mT [28], respectively. At the same time, a set of control experiments without MF treatment was set up.

The HRB400 steel bar with a diameter of 10 mm and a length of 120 mm was taken as the experimental object. A 3.5 wt. % sodium chloride solution concrete simulation solution is used as the test medium, and the composition is

shown in reference [29]. The rebar was cleaned by pickling, dried and weighed to record the initial mass m_0 of the rebar. The connection between the rebar and the wire was sealed using insulating tape and epoxy resin. The sample rebar was used as the electrode anode, the stainless steel was used as the electrode cathode, and the constant current power supply was connected in series. The current was accelerated for 7 days, and the constant current control is adopted. The current size was 50 mA. The corrosion test device of rebar under alternating MF was shown in Figure 2. At the beginning of energization, the current will fluctuate slightly due to the concentration polarization. The voltage of the potentiostat was adjusted in time to ensure that the current output value was constant. After energization, the current of the corrosion circuit was tested every day to ensure the accuracy of the test. After the end of the test, the rebar sample was taken out, the corrosion products on the surface of the rebar were removed, the corrosion morphology was observed, and the weight was weighed. The quality of the rebar after corrosion was m_1.

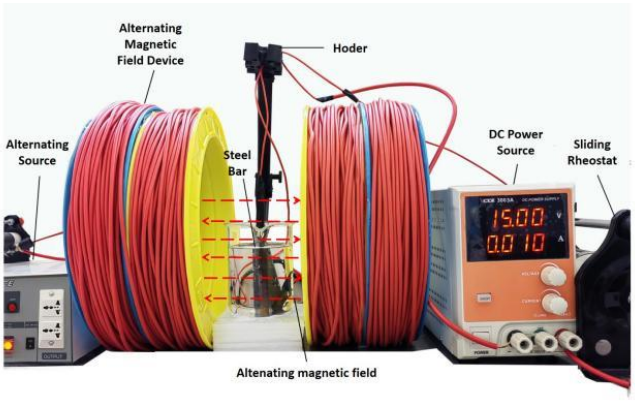

Figure 2. Steel corrosion test device under alternating MF

The HRB400 rebar with a size of Φ6mm and a length of 3 mm was used in the electrochemical test. The standard three-electrode system was used, in which the working electrode was rebar, the reference electrode was HgO, and the auxiliary electrode was Pt. The OCP, polarization curve (PC), and electrochemical impedance spectroscopy (EIS) were tested to analyze and evaluate the corrosion resistance of the sample. The operating temperature was 20±1°C. The accelerated electrochemical system under the action of alternating MF was shown in Figure 3.

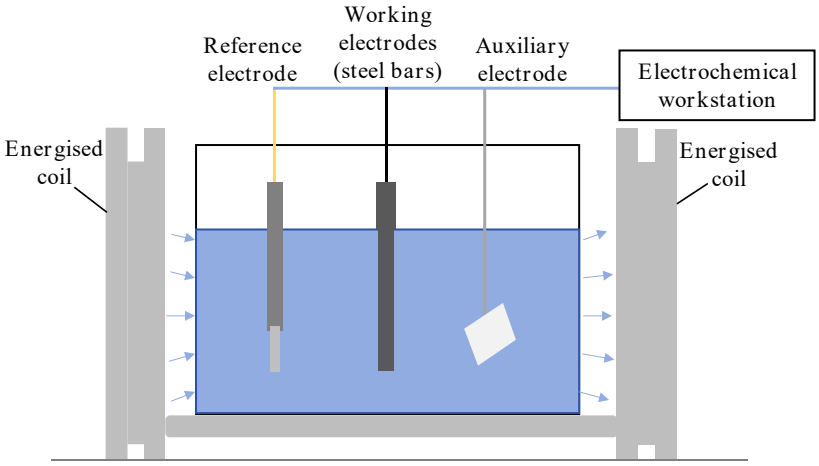

Figure 3. Accelerated electrochemical system under alternating MF

3. Results and Discussion

3.1. Accelerated Corrosion Test Results

Figure 4 shows the corrosion morphology of the rebar under different alternating MF. Figure 4 shows that in the absence of an external MF, the light yellow floc covered the entire rebar surface slowly and evenly over time. The amount of floc increased significantly in the presence of an external alternating MF, and the floc was mainly formed on the central axis of the coils on both sides of the rebar at the initial stage of corrosion. The corrosion products on both sides of the rebar at the central axis of the coil gradually spread in the direction perpendicular to the central axis over time and finally covered the entire rebar surface. The volume and formation rate of corrosion products increase with the intensity of the alternating magnetic induction, implying that the alternating MF accelerates the corrosion of the rebars.

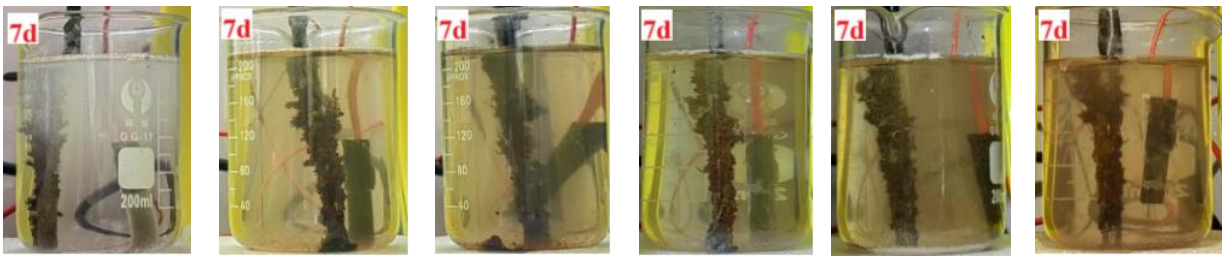

(a) 0 mT (b) 1 mT (c) 2 mT (d) 3 mT (e) 4 mT (f) 5 mT

Figure 4. The corrosion morphology of the rebar under different alternating MF

Figure 5 shows the color of the solution under different alternating MF. It can be seen that the color of the solution was light green without MF. As the intensity of the alternating magnetic induction increased, the color of the solution gradually changed to reddish brown. In the absence of the MF, the mass transfer between OH- generated by the cathode and Fe2+ generated by the anode is combined into a precipitate, and the main components in the solution are $Fe(OH)_2$ and $Fe(OH)_3$. The content of red rust (Fe_2O_3), black rust (Fe_3O_4), and $Fe(OH)_3$ in the solution increases. Under the MF of 5 mT, Fe is fully oxidized, and more oxides of high-valence Fe are produced, in which the proportion of reddish-brown Fe_2O_3 becomes higher. The magnetic ions and corrosion products are affected by the Lorentz force under the action of alternating MF, which changes the direction of mass transfer. The Fe_2O_3 and Fe_3O_4 initially adsorbed on the rebar surface move toward detachment, resulting in the corrosion products in the diffusion layer interface. The increased diffusion rate elevates the concentration of corrosion products in the solution, resulting in darker coloration.

(a) 0 mT (b) 1 mT (c) 2 mT (d) 3 mT (e) 4 mT (f) 5 mT

Figure 5. Colour of solutions in different alternating MF

The theoretical corrosion amount of rebar is:

$$\Delta m_0 = \frac{MI\Delta t}{Fn} = 1.749g \quad (1)$$

In the formula, M is the mass of Fe atom; I is the current, 10mA; t is the corrosion time, 7d; F is the Faraday constant; n is the number of electricity price.

The difference between the mass m_1 of the rebar after corrosion and its initial mass m_0 is Δm, as shown in Equation 2. Calculate the corrosion efficiency α, as shown in Equation 3:

$$\Delta m = m_1 - m_0 \quad (2)$$

$$\alpha = \frac{\Delta m}{\Delta m_0} \quad (3)$$

The data are shown in Table 1.

Table 1. The amount of rebar corrosion

B (mT)	Δm_0 (g)	Δm (g)	Relative Corrosion (g)	α (%)
0	1.749	1.57	0.179	89.77%
1	1.749	1.66	0.089	94.91%
2	1.749	1.66	0.089	94.91%
3	1.749	1.7	0.049	97.20%
4	1.749	1.72	0.029	98.34%
5	1.749	1.73	0.019	98.91%
Average	**1.749**	**1.673**	**0.076**	**95.67%**

According to Table 1, the actual corrosion value of the rebar is obtained and compared with the Faraday law-based theoretical value, as shown in Figure 6. The measured corrosion amount of rebars under the action of alternating MF is significantly lower than the Faraday law-based theoretical value. This is because a part of the current converts electrical energy into other forms of energy through charge transfer during the energized corrosion process, in which the anode and cathode generate gas, resulting in energy loss. The greater the magnetic induction strength, the higher the rebar corrosion amount and efficiency. The corrosion amount of rebar without MF is 1.57 g. The corrosion amount at 5 mT is 0.16 g higher, and the corrosion efficiency at 5 mT is 9.14% higher. This is consistent with previous research results [23]. From the analysis of the effect of MF force, the alternating MF mainly produces Lorentz force on Fe^{2+}, which leads to the non-uniform distribution of iron oxide, maintains the exposed area of the rebar surface, and promotes the dissolution of the anode Fe on the rebar surface. From a diffusion perspective, the Lorentz force deflects the Fe^{2+} perpendicular to the rebar surface, which accelerates the stirring and diffusion of Fe_3O_4 into the solution, resulting in a gradual deepening of the color of the solution. From the analysis of corrosion products, the deposition rate is slow. In the anodic reaction, Fe has enough space to release Fe^{2+} and transfer electrons outward, which improves the solubility and reactivity of Fe and reduces the corrosion resistance of the rebar.

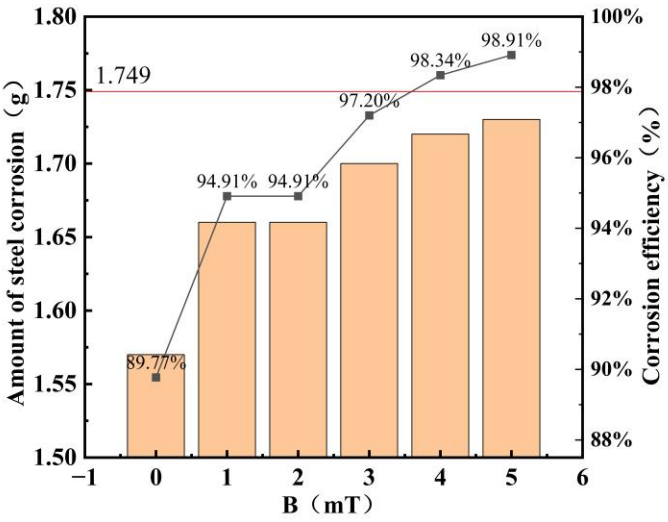

Figure 6. Corrosion amount and corrosion efficiency of rebars

3.2. Electrochemical Test under Energized Accelerated Corrosion State

The OCP of corroded rebars under different magnetic induction strengths for 7 consecutive days was shown in Figure 7. The OCP of the rebars shows a negative shift as the magnetic induction strength increases over the same number of days. This indicates that an alternating MF promotes corrosion of the rebars. This phenomenon may be closely related to the magneto-induced ion migration effect caused by the alternating MF. The alternating MF disturbs the Fe^{2+}/Cl^- plasma transmission path through the periodic Lorentz force, which leads to the enhancement of electrochemical polarization on the surface of the rebar, thereby reducing the activation energy barrier of the rebar corrosion and accelerating the local breakdown of the passivation film.

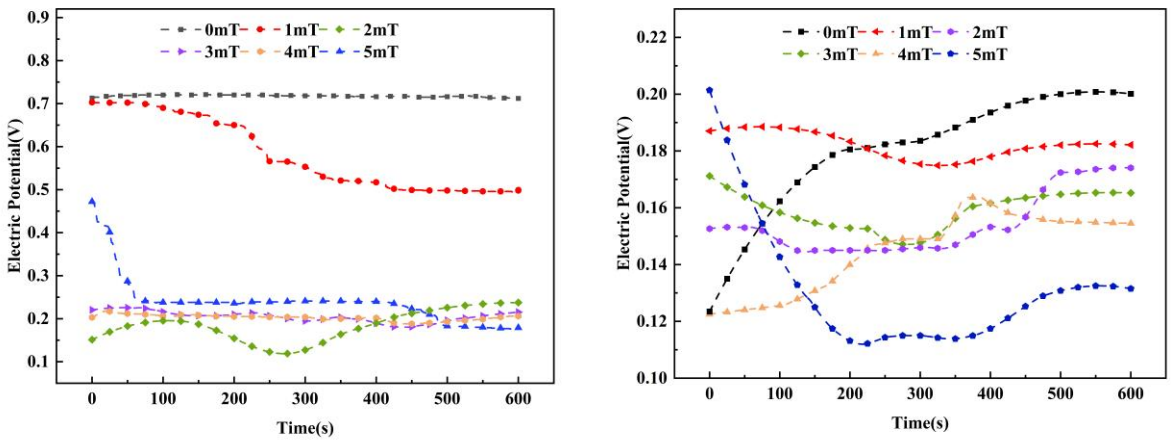

(a) 1d (b) 2d

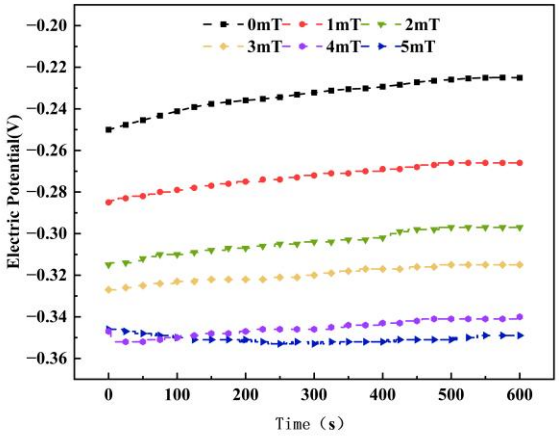

(c) 3d

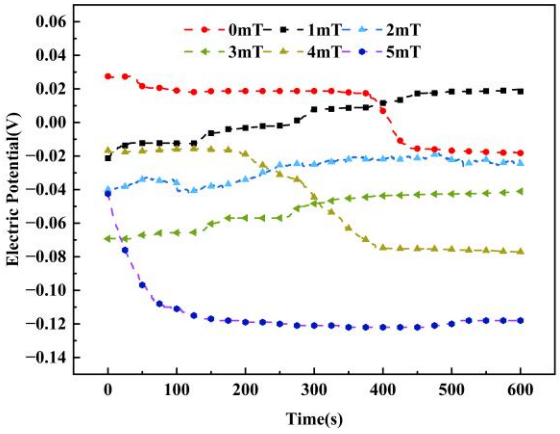

(d) 4d

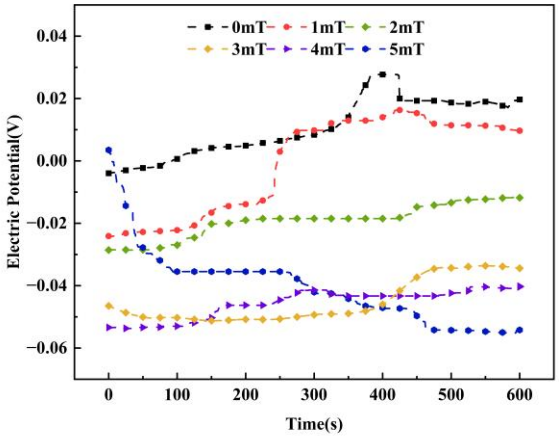

(e) 5d

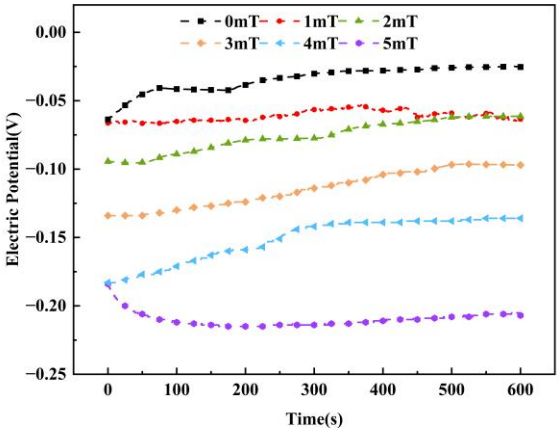

(f) 6d

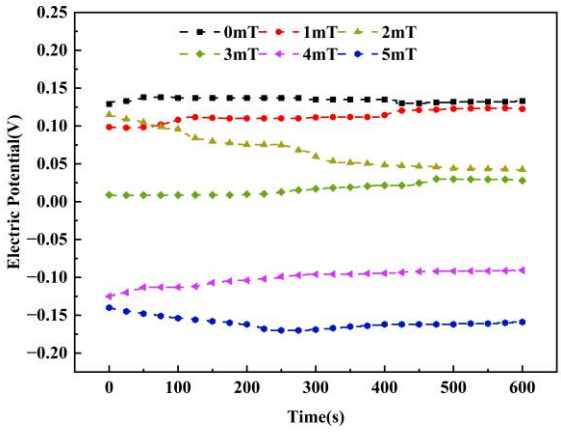

(g) 7d

Figure 7. The OCP of corroded rebars for 7 days under alternating MF

The OCP shifted by 937 mV in the absence of an MF and by 527 mV in the presence of a 5 mT MF over 7 days. It shows that the effect of MF on the OCP is smaller than that without MF. The reason may be that the anodic dissolution process dominated by current acceleration without MF continues to accelerate the dissolution of Fe^{2+}, resulting in the dissolution of passivation film and the increase of ion diffusion rate. Under the 5 mT alternating MF, Fe^{2+} is subjected to the Lorentz force to change the motion path, and a layer of corrosion products begins to form, whose physical barrier effect partially counteracts the enhancement effect of the MF on ion transport. In the late stage of rebar corrosion, the thickness and densification of the corrosion product layer increased significantly, which inhibited the efficiency of the MF in regulating the Fe^{2+} dissolution process. While the synergistic effect of the applied circuit-driven high-density current and the MF tended to saturate, the anodic dissolution rate is dominated by the diffusion limitation of the product

layer. The alternating MF accelerates the rupture of the passivation film by enhancing the local electrochemical polarization in the early stage of corrosion, while the product layer hinders the ion migration path in the later stage, resulting in a weakening of the MF effect.

When the alternating MF increased from 0 mT to 5 mT on the first day, the OCP shifted negatively by 534 mV, and the negative shift was 124 mV on the seventh day. It shows that the dynamic mechanism of rebar corrosion will be changed by an alternating MF. According to the magneto-hydrodynamic effect, the alternating MF disturbs the ion migration path through the periodic Lorentz force, which significantly enhances the transmission efficiency of Fe^{2+} at the initial stage of corrosion. However, with the thickening of the corrosion product layer, the regulation efficiency of MF on ion migration decreases due to the accumulation of corrosion products, which weakens the strengthening effect of MF on ion transport.

Figure 8 shows the electrochemical PC of the rebar corrosion process under an alternating MF of 0 mT to 5 mT. As can be seen from the PC of the rebars in Figure 8 under the action of an alternating MF for different lengths of time, the overall trend of the anodic PC on the first day of corrosion is very different from the PC in the middle and late stages of corrosion. On the first day without MF, there are two troughs in the anodic branch of the PC at -464 mV and -100 mV, respectively, which can be explained as the incomplete dissolution of the passive film on the surface of the rebar corresponding to the trough in the low potential area. At low potential, Cl^- invades the weak area of the passive film, causing local active dissolution, resulting in a temporary increase in current density and a decrease due to the repair of the passive film. The trough in the high-potential region is caused by the breakdown of the passivation film. When the polarization potential exceeds the critical value, the Fe^{3+} oxide (such as Fe_2O_3) in the passivation film is further oxidized to soluble FeO_4^{2-}, resulting in the current density rising again and forming the second peak. In the middle stage of steel corrosion on the second day, the effect of the alternating MF becomes apparent once the anodic polarization curve has reached the passivation potential. This is demonstrated by an increase in magnetic induction strength and a shift in the passivation potential (E_{pp}) towards negative values, and the alternating MF reduces the energy threshold required for the rupture of the passivation film. With the extension of corrosion time from 3 d to 7 d, the difference of anodic PC under different magnetic induction intensities gradually decreases, which may be related to the formation of a dense covering layer of corrosion products (such as FeOOH and Fe_3O_4) on the surface of rebars, which weakens the regulation of MF on ion migration. In the later stage of rebar corrosion, the anodic PC under different alternating magnetic induction intensities tends to be consistent, indicating that the alternating MF has little effect on the over-passivation stage of the anodic reaction.

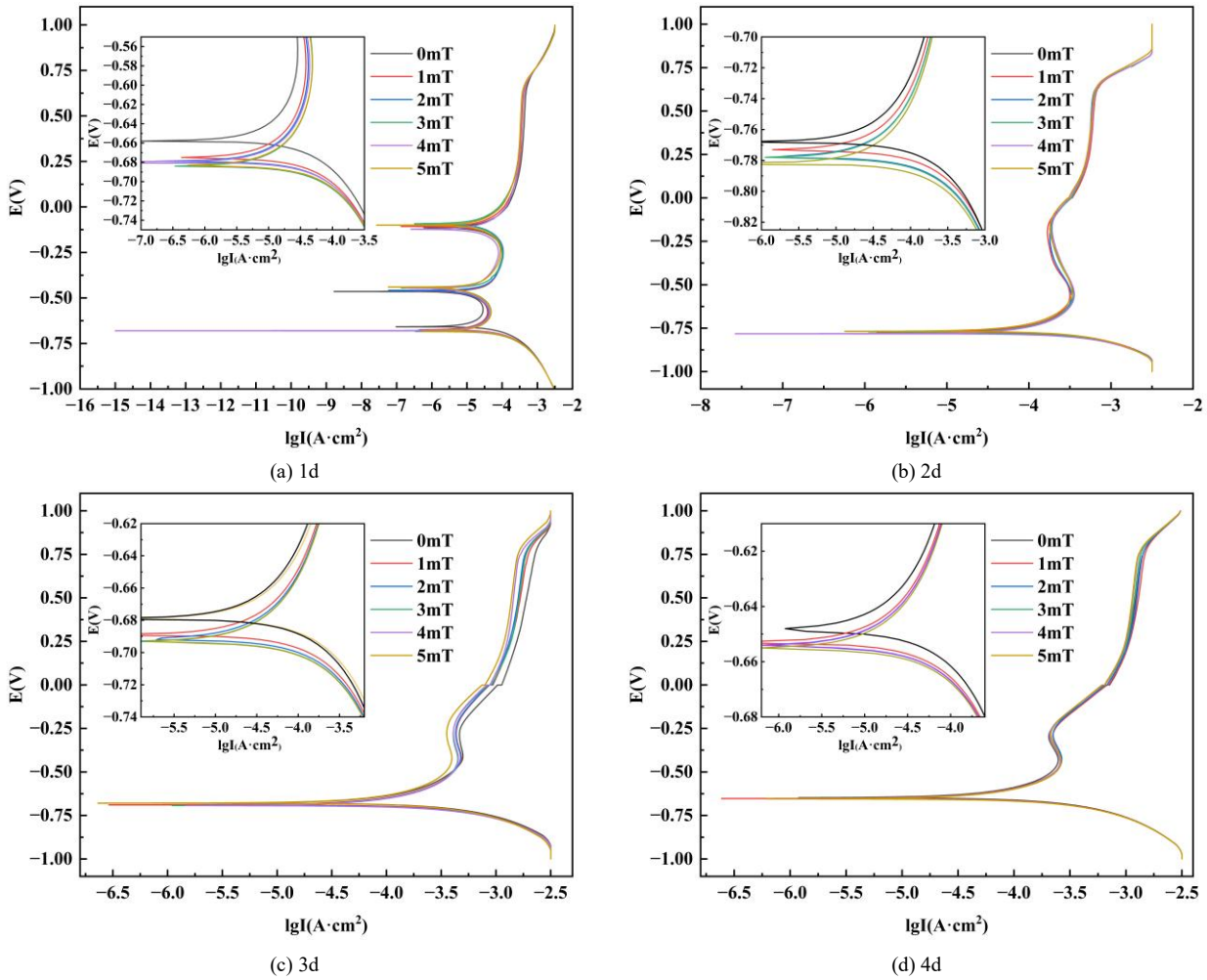

(a) 1d (b) 2d

(c) 3d (d) 4d

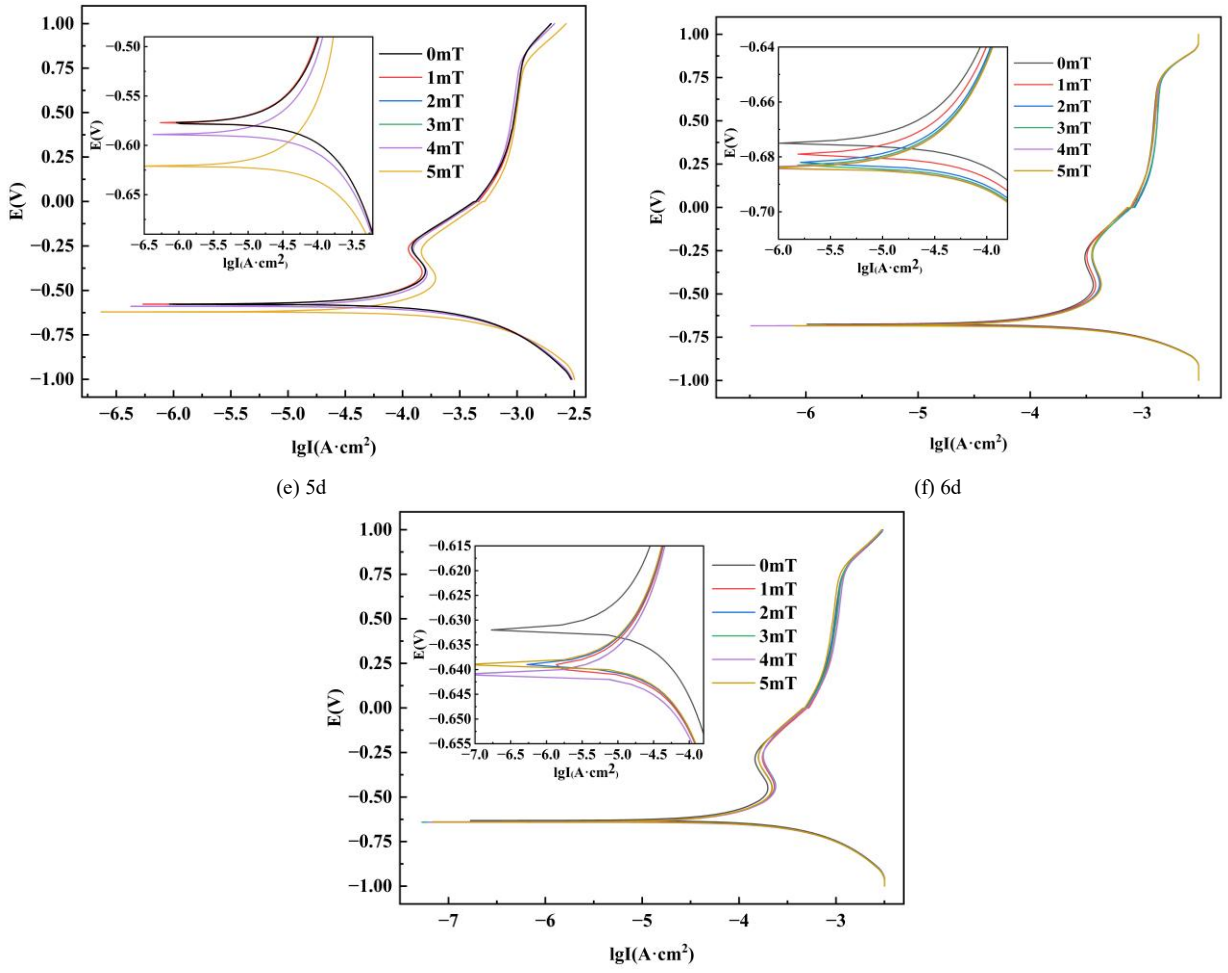

(e) 5d (f) 6d

(g) 7d

Figure 8. Polarization curves of 7d energized accelerated corroded rebars under alternating MF

The corrosion potential (E_{corr}) and corrosion current density (i_{corr}) of the corroded rebar under the action of alternating MF were analyzed through the PC test on each day, as shown in Figure 9. Under the influence of an alternating MF, an increase in the intensity of magnetic induction causes the E_{corr} of the rebar to shift gradually towards negative values and the i_{corr} to increase, implying that the alternating MF accelerates corrosion. In the initial stage of rebar corrosion, the corrosion potential drop or slow drop is accompanied by the phenomenon that the i_{corr} increases sharply or slowly. When the rebar is in the repassivation stage, the i_{corr} decreases slowly and then increases. The E_{corr} drops sharply, indicating that the passive film begins to dissolve. At this time, the localized corrosion micro-cell formed by Cl^- invasion is activated, which may be related to the electrochemical reaction rate in the Cl^- aggregation area. The corrosion potential slowdown process corresponds to the dynamic competition between the corrosion expansion of the active point and the repair of the passive film. At this time, the i_{corr} increases slowly in a stepwise manner. When the Cl- concentration is lower than the critical value, the repassivation shows a rapid decrease after a sudden increase in i_{corr}, corresponding to the formation process of a new passivation film under cathodic protection. In the process of film formation in the depassivation-repassivation cycle, i_{corr} increases suddenly only when depassivation occurs again. The change of potential only reflects the state of passive film, while the increase of i_{corr} directly characterizes the irreversible process of continuous dissolution of the steel matrix. In general, the i_{corr} value increases with the intensity of the alternating magnetic induction. When magnetic induction strength increases from 0 mT to 5 mT, the average increase in i_{corr} is 4.9%, which may be related to the acceleration of the electron transfer rate of the Fe^{2+}/Fe^{3+} oxidation-reduction reaction by MF.

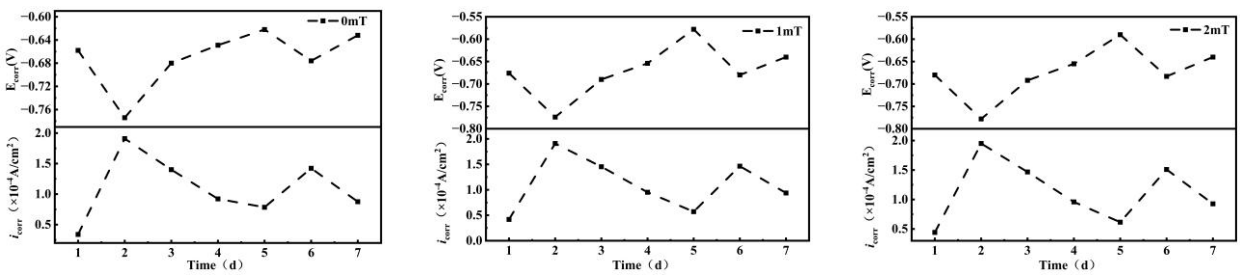

(a) 0 mT (b) 1 mT (c) 2 mT

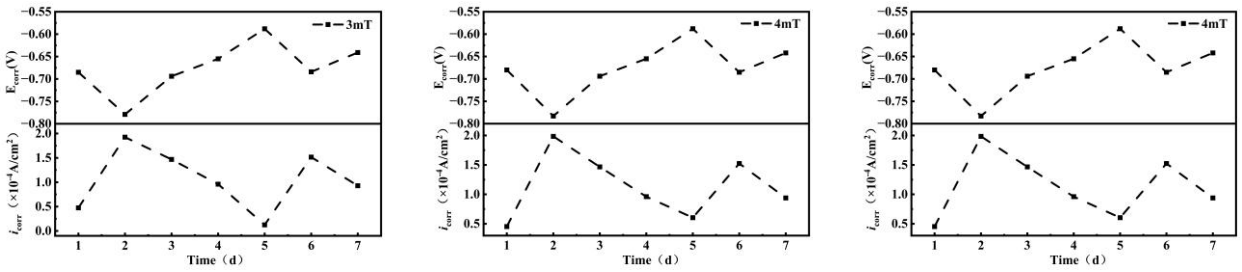

(d) 3 mT (e) 4 mT (f) 5 mT

Figure 9. The variation trend of E_{corr} and i_{corr} with time under alternating MF

3.3. Electrochemical Test in Natural Corrosion State

The corrosion current density of rebars under energized conditions is significantly increased by the external electric field, and its synergistic effect with the alternating MF may further regulate the corrosion kinetics. Therefore, in this section, the OCP, dynamic PC, and EIS of rebars under the natural corrosion state of alternating MF are analyzed by electrochemical tests. Figure 10 shows the electrochemical system schematic diagram in a natural corrosion state under the influence of an alternating MF. In addition to the rebar without an external circuit series of stainless steel, the test process is consistent with the energized accelerated test.

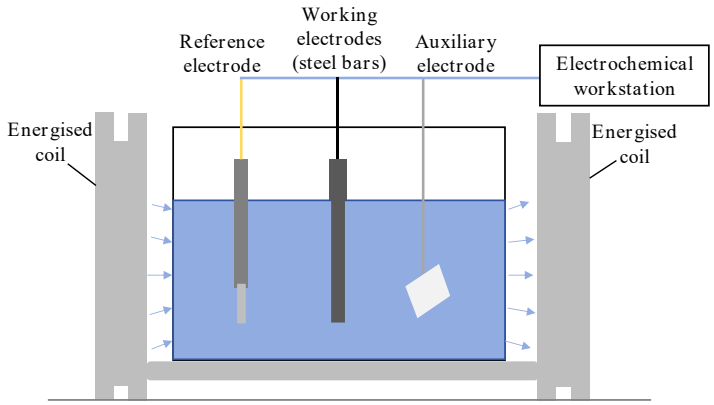

Figure 10. Electrochemical system of natural corrosion

The corrosion potential is shown in Figure 11, and the OCP of the rebar is significantly affected by the alternating MF. With the increase of the magnetic induction strength, the OCP of the rebar shows a negative shift trend. Without an MF, the OCP of the rebar fluctuates greatly in the early stage of immersion and tends to be stable until the 400s. This may be due to the instability of the passivation film on the rebar surface during the initial stages. Under the alternating MF of 1 mT, the OCP is slightly positively shifted, which is not much different from that of 0 mT. The negative shift in OCP increases as magnetic induction strength increases. The OCP of 5 mT is negatively shifted by 12 mV compared with that without MF. The effect of alternating MF on rebar corrosion is more obvious.

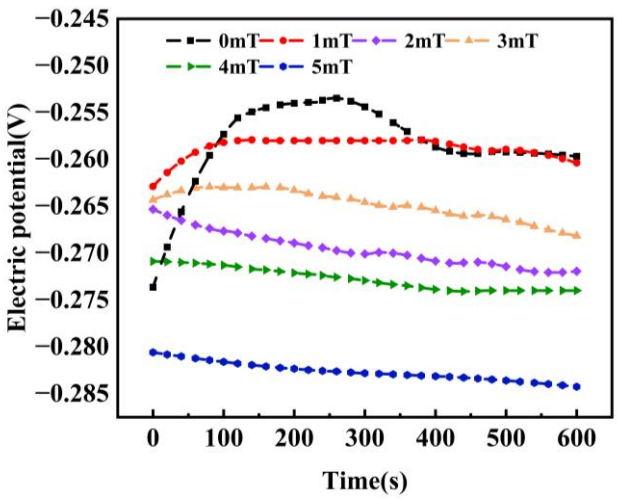

Figure 11. OCP of rebar

The PC test shows that the PC of the rebar in the simulated pore solution of concrete under an alternating MF can be obtained, as shown in Figure 12. The diagram makes it clear that the effect of the alternating MF on the cathodic PC is not obvious. The trend and range of the cathodic PC are essentially unchanged by the application of an MF, indicating that the alternating MF has no significant effect on the cathodic reaction mechanism. The characteristics of the anodic PC at the initial stage of polarization under the action of an alternating MF are essentially the same as those in the absence of an MF. The activation zone, passivation zone, and over-passivation zone appear consistently. The anode's Tafel slope is small, and there is no significant difference between the passivation zones of the rebar. The range of the passivation zones is essentially identical. When the potential reaches 8 mV, the rebar basically reaches the passivation zone, the passivation film begins to be destroyed, and the corrosion phenomenon intensifies again. This may be because the layer that forms on the rebar during the passivation stage makes the rebar more stable, and the current does not change with the potential. In the overpassivation stage, the passivation film is destroyed, the anodic reaction process on the surface of the rebar changes, and the corrosion is aggravated again. In addition to continuing to generate Fe^{2+}, the rebar also undergoes oxygen evolution and chlorine evolution reactions. At the same time, under certain conditions, the iron series ions of Fe^{3+} and Fe^{6+} are generated. In the anode pre-passivation stage, the dissolution range of anode Fe is roughly -854 mV to -25 mV without an MF, and the passivation potential is -708 mV. Exposure to a 5 mT alternating MF results in a lower passivation current density at the passivation potential, indicating that the passivation film on the rebars is more easily destroyed. Under different alternating MF, the dissolution range and passivation potential range of anode Fe are roughly consistent with those without MF, and then the rebar enters the passivation stage, and the passivation potential range is -8 mV~567 mV. The anodic PC in the passivation stage are basically the same, whether there is an MF or not. The current density increases sharply, and the rebar begins to depassivate.

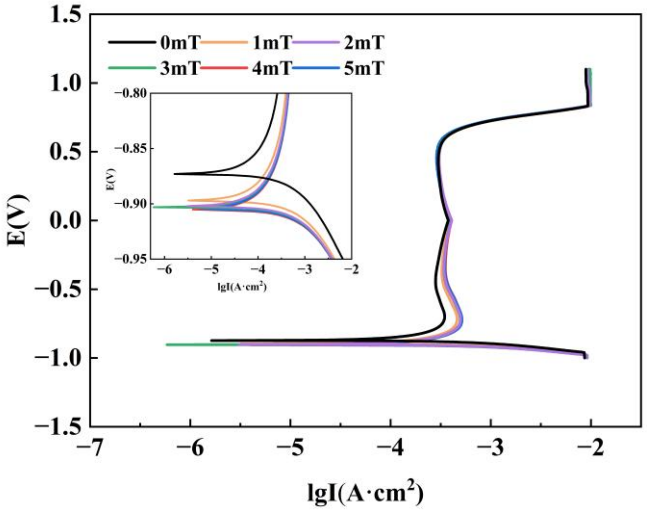

Figure 12. PC of rebar under alternating MF

The E_{corr} and i_{corr} of rebar in 3.5 wt. % NaCl concrete simulated pore solution under alternating MF were obtained by Tafel linear extrapolation method based on the PC obtained by electrochemical corrosion test. The corrosion rate of rebar is obtained. The known PC equation of rebar is [30]:

$$i = i_{corr}\left[exp\frac{2.3\Delta E}{\beta_a}\right] - exp\left(-\frac{2.3\Delta E}{\beta_c}\right) \quad (4)$$

In the formula, β_a is the anodic Tafel slope; β_c is the Tafel slope of cathode; ΔE is the polarization value.

The PC of the rebar has a strong anodic polarization zone and a cathodic polarization zone. The anodic current density (i_a) and the cathodic current density (i_c) can be expressed as:

$$i_a = i_{corr}exp\left(\frac{2.3\Delta E}{b_a}\right) \quad (5)$$

$$i_c = i_{corr}exp\left(-\frac{2.3\Delta E}{b_c}\right) \quad (6)$$

The corrosion rate v_{corr} is expressed by Equation 7:

$$v_{corr} = \frac{Mi_{corr}}{nF} \quad (7)$$

In the formula, M is the atomic mass of Fe, 56 g/mol; n is the number of anode transfer charge, take 2.

The corrosion rate is calculated according to Equation 7, as shown in Table 2.

Table 2. Dynamic parameters of PC of rebar

B (mT)	E_{corr} (V)	β_a (V/dec)	β_c (V/dec)	β_a/β_c	v_{corr} (g/m²·h)	i_{corr} (A/cm²)
0	-0.898	0.098	0.058	1.69	4.51918	0.472849714
1	-0.903	0.094	0.059	1.59	4.51918	0.475291448
2	-0.904	0.094	0.058	1.62	5.996263	0.478762361
3	-0.905	0.094	0.059	1.59	6.410606	0.481116222
4	-0.906	0.094	0.059	1.59	6.749733	0.481171615
5	-0.914	0.093	0.059	1.58	6.957371	0.48279643

The E_{corr} and i_{corr} can be obtained from Table 2, as shown in Figure 13. According to the experimental data in Table 2 and Figure 13, a negative shift trend in the corrosion potential of rebars is shown when an alternating MF is present, compared to when there is no MF. The negative shift amplitude increases with the magnetic induction strength (0-5 mT). This phenomenon is related to the acceleration of Fe^{2+} dissolution by MF and the enhancement of ion concentration gradient in local micro-area, which is consistent with the magnetohydrodynamic effect. From the perspective of Tafel slope, the regulation effect of alternating MF have a stronger effect on anode Tafel slope than cathode Tafel slope. The cathodic polarization process of rebar is basically influenced by an alternating MF in the same way as it is by a cathodic polarization process without a MF. The anode Tafel slope will change slightly in the presence of an alternating MF, while the cathode Tafel slope will remain essentially unchanged. This indicates that the process of mass transfer associated with the cathodic hydrogen evolution reaction is not significantly affected by the presence of an alternating MF. The ratio of the Tafel slope of the anode to the Tafel slope of the cathode is significantly deviated from 1. This indicates that the dissolution process of the anode metal is mainly controlled by activation energy, and the cathodic hydrogen evolution reaction is mainly mass transfer control. From the perspective of corrosion current density, increased magnetic induction strength leads to increased anode PC rebar corrosion current density, indicating poor passivation film stability and susceptibility to destruction.

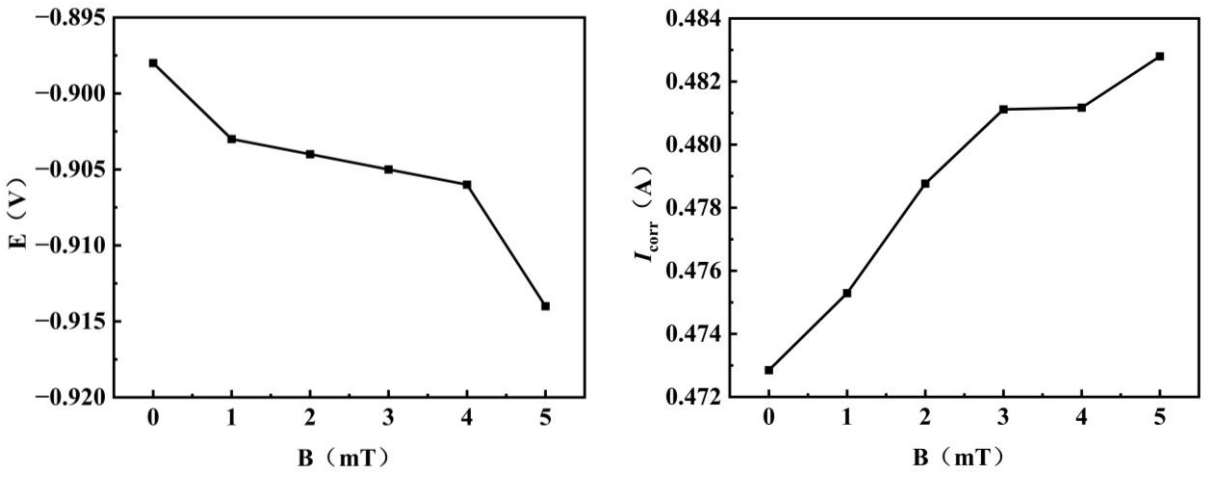

(a) E_{corr} (b) i_{corr}

Figure 13. E_{corr} and i_{corr} under different alternating MF

The Nyquist diagram of the rebar under the action of alternating MF is measured by electrochemical test, as shown in Figure 14. The diagram shows that the rebar's Nyquist diagram under the action of an alternating MF is approximately composed of a single arc. Let the solution resistance be R_s, the solution charge transfer resistance be R_t, and the actual part and the imaginary part satisfy Equation 8:

$$\left(Z_{Re} - R_s - \frac{1}{2}R_t\right)^2 + Z_{im}^2 = \left(\frac{1}{2}R_t\right)^2 \quad (8)$$

It can be seen from the Equation 8 that the Nyquist diagram is a circle with $(R_s + \frac{1}{2}R_t, 0)$ as the center and $\frac{1}{2}R_t$ as the radius. The R_t can be determined in advance using the radius of the capacitive arc in the impedance spectrum. Figure 14 shows that the arc radius of the electrochemical impedance curve without MF is the largest. An increase in magnetic induction strength results in a slight decrease in the radius of the capacitive arc. The alternating MF influences the charge transfer resistance of the electric double layer. The radius of the capacitive reactance arc is smallest at 5 mT. At this strength, the charge transfer resistance is reduced, the MF's effect on the passivation film is enhanced and the rebar's corrosion resistance is reduced. The actual and virtual components of the Nyquist diagram also decline with the rise of the magnetic induction strength, suggesting that the electrochemical reaction rate of the rebar speeds up.

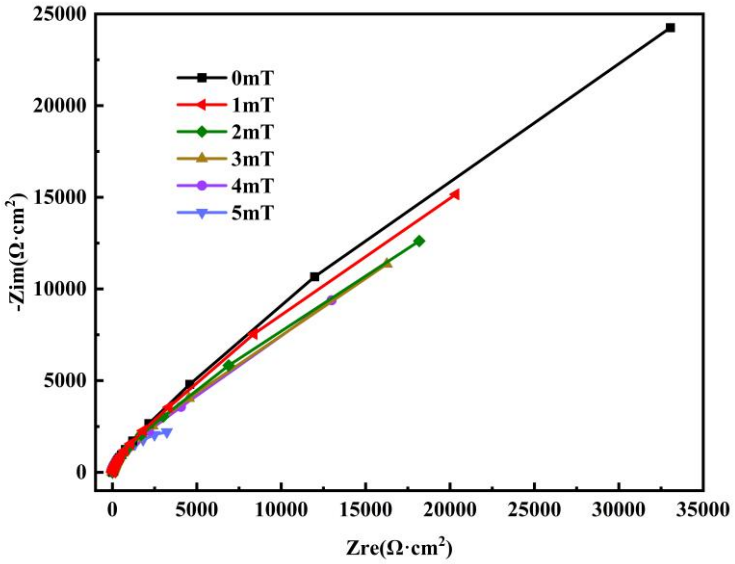

Figure 14. Nyquist diagram under alternating MF

Figure 15 shows the Bode relationship curve of the rebar under the influence of an alternating MF. When the frequency is approximately 102 to 103 Hz, it reflects the solution resistance. When the frequency is 10^{-1} to 10^{2} Hz, it reflects the double-layer capacitance. When the frequency is in the range of 10^{-2} to 10^{-1} Hz, it reflects the charge transfer resistance and charge transfer capacitance. The alternating MF mainly affects the impedance film values in the range of 10^{-2} to 10^{-1} Hz, indicating that the alternating MF affects the charge transfer resistance and charge transfer capacitance. The impedance modulus under an alternating MF with a frequency ranging from 10 Hz to 10 kHz is lower than that of 0 mT. The frequency-modulus curve gradually decreases as the magnetic induction strength of the alternating MF increases, indicating that the rebar's impedance and corrosion resistance decrease with increasing magnetic induction strength. These results are in line with the findings of the potentiodynamic PC test.

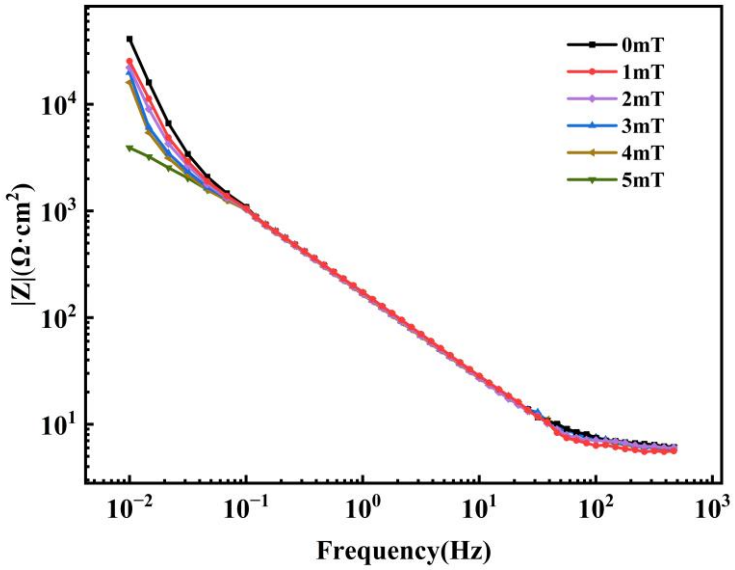

Figure 15. Bode-|*z*| *dia*gram

Figure 16 shows the Bode phase-angle relationship curve for the rebars under an alternating MF. It is clear that the Bode-phase diagram has only one characteristic peak, indicating that the impedance characteristic Nyquist diagram contains only a single capacitive arc. However, the phase angles corresponding to the characteristic peaks under different alternating MF are not significantly different. The phase angle of the alternating MF decreases within the 10 to 10^{3} Hz frequency range, indicating that the surface roughness of the rebar becomes higher after the field is applied. This is because the magnetic impurities in the solution are attracted to the surface of the rebar by an external alternating MF, causing the rebar to produce an adsorption force. An increase in magnetic induction strength enhances the adsorption force, making the impurity layer thicker and the rebar surface more uneven.

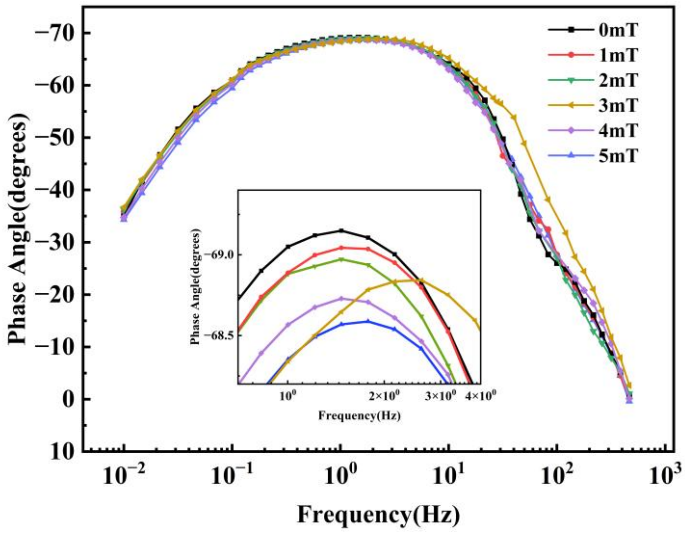

Figure 16. Bode-phase diagram

The Nyquist curve of EIS was fitted by Zview software, and the fitting equivalent circuit R(QR(QR)) of EIS was obtained, as shown in Figure 17. The equivalent components are the R_s, the resistance of the rebar surface oxidation product R_1, the R_t, and the capacitance of the oxidation product binding layer Q_1 and Q_2. The equivalent circuit consists of three units: solution resistance R_s, constant phase angle element Q_1 in parallel with oxidation product resistance R_1 on steel surface, and constant phase angle element Q_2 in parallel with electrochemical charge transfer resistance R_t. The constant phase angle element Q_1 is mainly the oxidation product capacitance, and the constant phase angle element Q_2 is mainly the charge transfer capacitance.

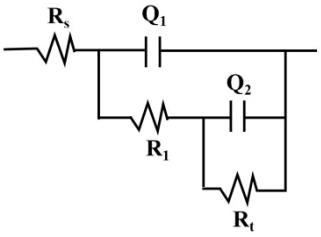

Figure 17. Equivalent circuit

According to the equivalent circuit in Figure 17, the electrochemical impedance spectrum of rebar is obtained. This is for different magnetic induction strength levels of an alternating MF. The results are shown in Table 3.

Table 3. The fitting results of EIS under alternating MF

B (mT)	*Rs* (Ω·cm²)	Q_1		R_1 (Ω·cm²)	Q_2		R_t (10^4Ω·cm²)
		Y_0 (10^{-5}Ω^{-1}·cm^{-2}·s^n)	n_1		Y_0 (10^{-5}Ω^{-1}·cm^{-2}·sn)	n_2	
0	5.653	0.0013102	0.824	3669	0.0039612	1.082	1730
1	6.11	0.0010339	0.876	690.3	0.00041641	0.888	3650
2	5.713	0.0010537	0.872	309	0.00045348	0.639	5431
3	5.947	0.0009234	0.897	286.3	0.00053004	0.719	6112
4	5.503	0.00096018	0.886	241.8	0.00049503	0.706	4542
5	4.924	0.0005482	0.969	62.03	0.00085706	0.708	6145

Table 3 shows that the R_1 on the surface of rebar decreases. This is due to an increase in alternating magnetic induction strength. The corrosion degree of rebar increases. This is due to an accelerated in the corrosion rate. Therefore, the effect of alternating MF is not conducive to the rust prevention of rebar. The above results are due to the increased Lorentz force caused by the alternating MF accelerating the diffusion rate of the magnetic ions and reducing the thickness of the electric double layer in the rebar corrosion electrochemical system, thereby promoting the corrosion process. In particular, the chloride ion concentration affects the stability of the passive film on the rebar surface, accelerating corrosion and increasing the fluctuation of oxidation product resistance.

4. Conclusions

This paper presents the design of an alternating MF test device. The corrosion morphology, corrosion rate, and corrosion product distribution of rebars under alternating MF were studied by using the accelerated corrosion method. The OCP, PC, and EIS were analyzed by electrochemical method to reveal the corrosion behavior mechanism and electrochemical corrosion characteristics of rebars under alternating MF. The results show that:

- The test of alternating MF on corrosion found that a higher magnetic intensity accelerated the diffusion of products in the solution. Measuring the corrosion of rebar showed that the 5 mT MF increased corrosion by 0.16 g and efficiency by 9.14%. The MF promoted rebar corrosion.
- The OCP of rebars under an alternating MF was analyzed. It was observed that, under the influence of an alternating MF, the E_{corr} of the rebar shifted negatively and the i_{corr} increased as the magnetic induction strength increased. The initial stage of corrosion exhibited a greater negative shift than the later stage. The PC analysis shows that, under an alternating MF, the E_{corr} and i_{corr} of rebars gradually shift negatively and increase with intensity. In the middle stage of rebar corrosion, the passivation potential E_{pp} also shifts negatively. The difference in anodic PC under different magnetic induction strengths decreases gradually.
- Through analyzing the OCP of rebar in a natural corrosion state under an alternating MF, it was found that the effect of an alternating MF on corrosion was more obvious. The OCP of a 5 mT field was shifted negatively by 12 mV compared to a field without an MF. Polarization curve analysis showed that, at the same passivation potential, the passivation current density of the 5 mT alternating MF was lower than that of the field with no magnetic induction, and the rebar's passivation film was more easily destroyed. As the magnetic induction strength of the alternating MF increased, the E_{corr} of the rebar shifted negatively and the i_{corr} increased significantly, while the cathodic hydrogen evolution reaction's mass transfer mechanism remained largely undisturbed. EIS analysis shows that, as the magnetic induction strength of the alternating MF increases, the radius of the capacitive reactance arc decreases gradually. The phase angle moves downwards within the frequency range of $10\sim10^3$ Hz under the action of the alternating MF. Equivalent circuit fitting analysis revealed that the resistance of the oxidation products decreases with increasing alternating magnetic induction strength.

In summary, this study mainly discussed the effect of alternating magnetic induction strength on the corrosion behavior of rebars and clarified its mechanism. It should be pointed out that in practical engineering, rebars are affected by a variety of environmental factors, such as chloride ion diffusion behavior in concrete [31, 32]. In the future, a multi-field coupling model of the MF-chloride ion environment can be considered to be close to the actual working conditions.

5. Declarations

5.1. Author Contributions

Conceptualization, Y.J., Y.W., and Y.X.; methodology, Y.J., Y.W., and Y.X.; investigation, Y.J.; data curation, Y.J.; writing—original draft preparation, Y.X.; writing—review and editing, Y.W. All authors have read and agreed to the published version of the manuscript.

5.2. Data Availability Statement

The data presented in this study are available in the article.

5.3. Funding

This research was funded by National Natural Science Foundation of China (52209155); Hunan Natural Science Foundation (2023JJ30045).

5.4. Conflicts of Interest

The authors declare no conflict of interest.

6. References

[1] Prasad, N., Jain, S., & Gupta, S. (2019). Electrical Components of Maglev Systems: Emerging Trends. Urban Rail Transit, 5(2), 67–79. doi:10.1007/s40864-019-0104-1.

[2] Shi, J., Fang, W. S., Wang, Y. J., & Zhao, Y. (2014). Measurements and analysis of track irregularities on high speed maglev lines. Journal of Zhejiang University: Science A, 15(6), 385–394. doi:10.1631/jzus.A1300163.

[3] Felez, J., Vaquero-Serrano, M. A., Portillo, D., Antunez, S., Carcasi, G., Nocita, A., Schultz-Wildelau, M., Parrotta, L. A., Fasano, G., & Proietti, P. (2025). A New Concept of Hybrid Maglev-Derived Systems for Faster and More Efficient Rail Services Compatible with Existing Infrastructure. Sustainability (Switzerland), 17(11), 5056. doi:10.3390/su17115056.

[4] Gaspar, J., Cruz, T., Lam, C. T., & Simoes, P. (2023). Smart Substation Communications and Cybersecurity: A Comprehensive Survey. IEEE Communications Surveys and Tutorials, 25(4), 2456–2493. doi:10.1109/COMST.2023.3305468.

[5] Kryukov, A., Suslov, K., Seredkin, D., Voronina, E., Batukhtin, A., Ilyushin, P., & Shepovalova, O. (2025). Reducing electromagnetic pollution of the environment at main railway facilities. Management of Environmental Quality, 234. doi:10.1108/MEQ-04-2025-0234.

[6] Abreu Silveira, C., Da Costa, C., Costa E Silva, R., Soares, L., & Pugliese Guimaraes, J. (2006). Electromagnetic Environment Measurement under Steady-State Conditions in Utility Substations. 2006 IEEE/PES Transmission & Distribution Conference and Exposition: Latin America, 1–6. doi:10.1109/tdcla.2006.311511.

[7] Guo, B., Zhang, P., Jin, Y., & Cheng, S. (2008). Effects of alternating magnetic field on the corrosion rate and corrosion products of copper. Rare Metals, 27(3), 324–328. doi:10.1016/S1001-0521(08)60138-2.

[8] Xing, Y. C., Sun, Z. B., Han, Y. Q., & Zhang, D. X. (2025). Influence of alternating magnetic field on corrosion and microstructure of 2205 duplex stainless steel welded joints. Journal of Iron and Steel Research International, 32(5), 1341–1355. doi:10.1007/s42243-024-01398-w.

[9] Ma, Y., Peng, A., Su, X., Wang, L., & Zhang, J. (2021). Modeling Constitutive Relationship of Steel Bar Removed from Corroded PC Beams after Fatigue Considering Spatial Location Effect. Journal of Materials in Civil Engineering, 33(4), 4021019. doi:10.1061/(asce)mt.1943-5533.0003644.

[10] Peng, A., Ma, Y., Wang, L., & Zhang, J. (2023). Fractographic Analysis and Particle Filter-Based Fatigue Crack Propagation Prediction of Q550E High-Strength Steel. Journal of Materials in Civil Engineering, 35(11), 4023406. doi:10.1061/jmcee7.mteng-16335.

[11] Peng, A., Ma, Y., Huang, K., & Wang, L. (2024). Digital twin-driven framework for fatigue life prediction of welded structures considering residual stress. International Journal of Fatigue, 181, 108144. doi:10.1016/j.ijfatigue.2024.108144.

[12] Yang, J. (2019). Theoretical and experimental investigation on durability of concrete structures in coastal substation. Master's thesis, Tongfang Knowledge Network (Beijing) Technology Co., Ltd, Beijing, China. doi:10.27135/d.cnki.ghudu.2019.000790.

[13] Li, W., Yang, J., & Jiang, P. (2023). Study of Reinforcement Corrosion in Reinforced Concrete Structures under the Action of Magnetic Fields. Total Corrosion Control, Tongfang Knowledge Network (Beijing) Technology Co., Ltd., Beijing, China. doi:10.13726/j.cnki.11-2706/tq.2023.09.087.05.

[14] Liu, Y., Yang J., & Jiang P. (2023). Study on Corrosion of A3 Carbon Steel in Concrete Simulation Solution Under AC. Total Corrossion Control, Tongfang Knowledge Network (Beijing) Technology Co., Ltd., Beijing, China. doi:10.13726/j.cnki.11-2706/tq.2023.09.082.05.

[15] Ye, X., Yang, J., Yang, W., Chen, T., Li, W., & Liu, Y. (2025). Theoretical and experimental study on the effect of magnetic field on the amount of steel bars corrosion. Corrosion Science, 255, 113082. doi:10.1016/j.corsci.2025.113082.

[16] Srivastava, K., & Nigam, N. (1988). Protection of mild steel in sulphuric acid by magnetic fields. British Corrosion Journal, 23(3), 172–175. doi:10.1179/000705988798270758.

[17] Chiba, A., Wu, W. C., & Terashita, A. (1996). Influence of the magnetically treated 3% sodium chloride solution on the corrosion of iron. Journal of Materials Science, 31(14), 3821–3825. doi:10.1007/BF00352797.

[18] Chiba, A., Tanaka, N., Ueno, S., & Ogawa, T. (1992). Inhibition by Magnetic Fields of the Corrosion of Iron in Sodium Chloride Solution. Zairyo-to-Kankyo, 41(5), 287–292. doi:10.3323/jcorr1991.41.287.

[19] Sagawa, M. (1982). Effect of a Local Magnetic Field on the Dissolution of Copper and Iron in Nitric Acid Solution. Transactions of the Japan Institute of Metals, 23(1), 38–40. doi:10.2320/matertrans1960.23.38.

[20] Costa, I., Oliveira, M. C. L., De Melo, H. G., & Faria, R. N. (2004). The effect of the magnetic field on the corrosion behavior of Nd-Fe-B permanent magnets. Journal of Magnetism and Magnetic Materials, 278(3), 348–358. doi:10.1016/j.jmmm.2003.12.1320.

[21] Choi, J. K., Ohtsuka, H., Xu, Y., & Choo, W. Y. (2000). Effects of a strong magnetic field on the phase stability of plain carbon steels. Scripta Materialia, 43(3), 221–226. doi:10.1016/S1359-6462(00)00394-8.

[22] Sato, A., Ogiwara, H., Miwa, T., & Nakabayashi, S. (2002). Influence of high magnetic field on the corrosion of carbon steel. IEEE Transactions on Applied Superconductivity, 12(1), 997–1000. doi:10.1109/TASC.2002.1018568.

[23] Ang, L. Y., Othman, N. K., Jalar, A., & Ismail, I. (2016). The Effect of Magnetic Field on Corrosion Inhibitor of Copper in 0.5 M HCl Solution. Procedia Chemistry, 19, 222–227. doi:10.1016/j.proche.2016.03.097.

[24] Wei, Z. (2009). Study on durability of concrete structure in magnetic field environment. Master's thesis, School of Civil Engineering, Tongji University, Shanghai, China. doi:10.7666/d.y1449555.

[25] Memon, S. A., & Fromme, P. (2014). Stray Current Corrosion and Mitigation: A synopsis of the technical methods used in dc transit systems. IEEE Electrification Magazine, 2(3), 22–31. doi:10.1109/MELE.2014.2332366.

[26] Ogunsola, A., Sandrolini, L., & Mariscotti, A. (2015). Evaluation of stray current from a DC-electrified railway with integrated electric-electromechanical modeling and traffic simulation. IEEE Transactions on Industry Applications, 51(6), 5431–5441. doi:10.1109/TIA.2015.2429642.

[27] Dolara, A., Foiadelli, F., & Leva, S. (2012). Stray current effects mitigation in subway tunnels. IEEE Transactions on Power Delivery, 27(4), 2304–2311. doi:10.1109/TPWRD.2012.2203829.

[28] Zhang, Y., Fan, L., Liu, Z., Ma, D., Luo, H., Yang, X., Song, L., & Li, X. (2021). Effect of Alternating Magnetic Field on Electrochemical Behavior of 316L and TA2 in Simulated Seawater. Journal of Materials Engineering and Performance, 30(12), 9377–9389. doi:10.1007/s11665-021-06131-2.

[29] Choi, Y. S., Kim, J. G., & Lee, K. M. (2006). Corrosion behavior of steel bar embedded in fly ash concrete. Corrosion Science, 48(7), 1733–1745. doi:10.1016/j.corsci.2005.05.019.

[30] Zhou, B., Gu, X., Guo, H., Zhang, W., & Huang, Q. (2018). Polarization behavior of activated reinforcing steel bars in concrete under chloride environments. Construction and Building Materials, 164, 877–887. doi:10.1016/j.conbuildmat.2018.01.187.

[31] Peng, J., Cheng, X., Yang, Y., & Xiao, J. (2025). Chloride transport in concrete subjected to multiple cracks under drying-wetting cycles. Construction and Building Materials, 470, 140559. doi:10.1016/j.conbuildmat.2025.140559.

[32] Cheng, X., Peng, J., Cai, C. S., & Zhang, J. (2020). Experimental Study on Chloride Ion Diffusion in Concrete under Uniaxial and Biaxial Sustained Stress. Materials, 13(24), 5717. doi:10.3390/ma13245717.